Observation of different mass removal regimes during the laser ablation of an aluminium target in air

Gabriele Cristoforetti,* Stefano Legnaioli, Vincenzo Palleschi, Elisabetta Tognoni and Pier Alberto Benedetti

The mass removal mechanisms occurring during the ablation of an aluminium target, induced by a Nd:YAG laser at $\lambda = 1064$ nm in air, were investigated in the fluence range between 1.5 and 840 J cm^{-2}. The spectroscopic analysis of the plasma emission allowed the calculation of the plasma thermodynamic parameters and an estimation of its atomized mass. Conversely, microscopic analysis of the craters allowed the calculation of the hole volume and the quantification of the material accumulated in the rim around it, as well as a qualitative inspection of the craters profile and appearance. The trends of line intensity, of the atomized plasma mass and of the crater volumes with laser fluence suggest the identification of four laser fluence ranges, where a different role of background gas is played and different mass removal mechanisms seem to occur. A complex picture is drawn where vaporization, melt displacement, melt expulsion and phase explosion take place at different laser fluences.

Introduction

Laser ablation of materials is used in a variety of applications, including micromachining, nanoparticle production, pulsed laser deposition, chemical analysis and surgery. However, because of the complex interplay of the matrix, ambient and experimental parameters, it is very difficult to draw an accurate picture of the process, which fits adequately the observations in all the situations. Most of the models presented in the literature tackle the issue of ablation in vacuum or at a low pressure background gas,[1-3] where the process is simplified by the absence of interactions between the laser beam and the induced plasma with the ambient gas atoms.

This approach is useful in some applications, as pulsed laser deposition, but is not appropriate in many others cases, such as laser ablation-inductively coupled plasma, typically occurring in helium or argon at 1 atm, or laser induced breakdown spectroscopy often performed in air at 1 atm. In these cases, striking differences in both the ablation stage and in the subsequent plume dynamics are evident with respect to ablation in vacuum or at low gas pressure.

The influence of the background gas on the dynamics of the plume has been studied by Monte Carlo simulations[4,5] (again at low gas pressures, usually at a few hundreds of Pascals) and by modelling.[6,7] However, in these works, the laser ablation process is not considered, assuming an initial amount of vaporized mass according to the experimental results.

The complete issue has been recently tackled by Chen et al.,[8] who presented a model including both the ablation and the subsequent plume expansion stages, which accounts also for background gas effects up to the atmospheric pressure. In a subsequent work, the same group applied the model for analysing the effect of several background gases on the laser ablation process;[9] their theoretical model, however, fits only partially the results obtained experimentally.

Hence, up to now, the mechanisms arising during the laser ablation stage and the parameters affecting such a process are mainly investigated experimentally by using different approaches, such as spectroscopic analysis of plasma emission, study of the residual craters in the target, imaging of plasmas or shock waves, time-of-flight measurements, laser beam deflection technique or other methodologies.

A complex picture of laser ablation can be drawn, where, for high enough laser irradiances, drilling may be produced on the surface by four different mechanisms, occurring disjointedly or simultaneously, i.e. vaporization, melt displacement, melt splashing and phase explosion.[10]

Vaporization of target surface is dominant at very low fluence values, where melt splashing is still negligible and phase explosion can be excluded. The mass removal rate, governed by the Hertz-Knudsen equation, initially increases with the surface temperature (and then with laser energy) but rapidly saturates because of the progressive increase of the inverse re-condensation process. At higher fluences, pressure gradients in the molten pool can induce displacement or even expulsion of liquid metal. The driving force may be internal, e.g. deriving from inhomogeneous vaporization of multi-element materials, resulting mainly in explosive melt-expulsion in the form of droplets, or may be external, e.g. produced by vapour recoil or plasma pressure, resulting in lateral melt displacement and eventually expulsion.[11] This second mechanism is mainly responsible for the melt accumulation across the borders of the hole. If the irradiation is strong enough to rapidly heat the sample leading the melting pool near the thermodynamic critical state, explosive boiling can also occur resulting in a considerable ejection of both

Applied Laser Spectroscopy Laboratory, Institute for Chemical-Physical Processes, Research Area of National Research Council, Via G. Moruzzi, 1, 56124 Pisa, Italy. E-mail: gabriele@ipcf.cnr.it; Fax: +39-050-3152230; Tel: +39-050-3152222

vapour and molten material.[12] In this case, the superheated metal experiences large density fluctuations, generating vapour bubbles which rapidly expand and cause the violent ejection of molten liquid. Another theoretically possible mechanism of mass removal is normal boiling, consisting of the formation of heterogeneously nucleated bubbles which diffuse towards the outer surface and may escape from the melting pool. However, detailed calculations (*e.g.* see Kelly and Miotello[13]) on bubble diffusion showed that such a mechanism is impossible for laser pulses shorter than ∼1 μs.

The relevance of the above mechanisms and their irradiance thresholds are currently under debate and depend on several parameters, mainly on the material properties and on the effective laser irradiance impinging on the target;[14] in turn, this latter parameter is strongly affected by the background gas composition and pressure, which therefore have a strong influence on the mass removal mechanism occurring.

The effect of the background gas on the laser vaporization and excitation processes were investigated by Iida[15] and Sdorra and Niemax[16] with spectral measurements and with direct measurements of vaporized material weight and crater dimensions. Their works, considering laser ablation occurring in several ambient gases at different pressures, highlight a strong influence of the ambient gas conditions on the laser-matter coupling and thus in the amount of material vaporized. In particular, the partial absorption of the laser pulse by the plasma formed in front of the target, a mechanism usually named "plasma shielding", seems to be strongly affected by the background gas. In the plasma shielding phenomenon, the laser photons are absorbed in the initial plume by inverse bremsstrahlung and photoionization, resulting in an increase of plasma temperature and in a reduction of the amount of sample vaporized. The influence of background gas atoms in this process is also testified by the reduction of the vaporized mass and by the growth of the plasma temperature with the increase of the environmental gas pressure.

Also, the dynamics of the vaporized mass is obviously strongly affected by the background gas; the plume expansion at high gas pressures is slower, resulting in a slower cooling of the plasma,[17] and the shock wave produced is stronger.

The plasma dynamics should not be considered separately from the laser ablation stage, because the two processes are strictly correlated. At early times, the plasma formation and the shock wave development are linked to each other, since the shock wave is fed by part of the laser pulse energy absorbed in the plasma through a laser supported detonation regime. On the other hand, the shock wave, during its expansion, heats and often ionizes the atoms encountered, then increasing the plasma dimensions. In turn, the increase of plasma dimensions affects the laser absorption and the amount of vaporized matter.

The correlation of shock wave dynamics and ablation rate has been observed by Stauter *et al.*,[18] who described the ablation process as a "plasma mediated ablation". In the case of low fluence regime, *i.e.* lower than 10 J cm^{-2}, a linear relationship between the ablation rate and the shock wave energy was found. Such a result is expected, since the shock wave energy is proportional to the energy absorbed by the plasma which, in turn, is proportional to the amount of vaporized material. At higher fluences, in case of irradiation with 1064 nm Nd:YAG

laser, a different behaviour was observed, associated to a lower ablation rate and to a stronger plasma shielding.

It is then expected that the presence of background gas at high pressure, through the plasma shielding effect, strongly influences the mechanisms of mass removal and their thresholds: on one hand, melt splashing is favoured by the formation of the hot high-pressure plasma, on the other, phase explosion is hindered by the reduction of the effective irradiance on the target.

To our knowledge, a complete study of the transitions between different mass removal regimes, during the laser ablation in air is still missing.

In this work, this study has been attempted by using an aluminium target and a Nd:YAG laser, emitting in the fundamental wavelength (λ = 1064 nm), whose pulse energy ranged from 0.3 up to 270 mJ. Both the spectroscopic study of laser induced plasmas and the direct analysis of residual craters were done, and the results were compared and discussed.

Experimental

The plasma was induced on the aluminium surface by focusing a Q-switched Nd:YAG laser (Lumonics HY 100), operating at 1064 nm in 10 ns pulses. The experiment was performed in air at atmospheric pressure. The beam was focused perpendicularly to the target surface by means of a 100 mm focal length lens; however, the lens to sample distance was set 5 mm less than the lens focal length, in order to avoid the air breakdown in front of the target and to improve the stability of the plasma.

The laser pulse energy, measured by means of a Scientech thermopile, was varied in the range between 0.5 and 270 mJ, corresponding to fluences respectively between 1.5 and 840 J cm^{-2} (irradiances between 1.5×10^8 W cm^{-2} and 8.4×10^{10} W cm^{-2}). The range of pulse energies between 0.5 and 4 mJ were obtained by using optical filters, because in the low energy range the laser operation is characterized by a poor reproducibility.

The sample was constituted by an almost pure aluminium (>99%) target, placed on a X–Z axis motorised micrometric stage for positioning. The target surface was previously polished with micro-fine sandpaper and cleaned with alcohol, to increase the reproducibility of measurements.

Since the atomized ablated mass (scaled by an arbitrary constant) is calculated from the spectra acquired, it is essential to reduce the uncertainty of the observed signal due to the different spatial emissivity distribution for different laser energies. For this purpose, the space-integrated LIBS signal was collected through an optical quartz fibre (diameter = 1 mm, N.A. = 0.22), placed at 45° with respect to the laser beam axis at a 3 cm distance from the target surface.

The optical signal was then sent to an Echelle spectrometer (Multichannel Instrument) coupled with an intensified CCD camera (effective λ/Δλ = 5000), which provided for each acquisition a full spectrum in the range between 200 and 900 nm. All the acquired spectra were rescaled by the curve of spectral efficiency of the detection system, which was calculated by means of a deuterium-halogen calibrated light source by Avantes Inc.

In all the measurements, an acquisition delay time of 1 μs with respect to the laser pulse was chosen in order to allow the decay of continuum, due to Bremsstrahlung radiation and free–bound

This journal is © The Royal Society of Chemistry 2008

J. Anal. At. Spectrom., 2008, **23**, 1518–1528 | 1519

electronic recombination. An acquisition gate of 1 μs was also chosen, which guaranteed well visible emission signals in all the different experimental conditions analysed, but still allowing a meaningful calculation of the spatially integrated thermodynamic parameters of the plasma.

In order to reduce the spectral fluctuations, a series of 20 laser pulses was averaged for each measurement, at a repetition rate of 2 Hz.

The size and shape of the craters obtained at different laser energies were evaluated using a ViCo (Biomedica Mangoni and Nikon Instruments, Italy) Video-Confocal Microscope (VCM). In VCM an arc lamp is used as a multi-point illumination source and a CCD camera as an image detector. Confocal capabilities are guaranteed by an original processing method.[19] Depending on needs, reflectance and depth imaging can easily be attained.[20]

For each crater, a stack of high-resolution optical sections were collected at steps of 2 to 5 μm, depending on crater depth, along the focal axis. A dry objective (Nikon 20X, 0.50 N.A.) was employed in all measurements. Depending on the actual crater depth, the overall range scanned along the focal axis was between 30 and 80 μm.

Starting from image stacks, the extended focus image of each crater is obtained by calculating the maximum projection of the reflectance signal from the set of focal sections. Moreover, a depth map or a 3D profile of the crater surface can also be obtained.

Results

Line intensity behaviour

Space-averaged emissions from laser-induced plasmas were acquired at different laser pulse energies, ranging from 0.5 mJ up to 270 mJ, corresponding to a range of fluences between 1.5 and 840 J cm^{-2}.

All the line intensities values used in the following were calculated by integrating the spectrum along the line profile and by subtracting the background component, by means of a fitting procedure.

A typical trend observed in line intensity with respect to laser fluence is reported in Fig. 1a for Al I emission at 305.0 nm and Al II emission at 281.6 nm. A similar behaviour was found for the other atomic and ionic lines of aluminium visible in the spectra. It should be noted that other stronger lines (*e.g.* Al I 394.4 nm and 396.1 nm), which were not plotted because they were strongly self-absorbed at moderate and high fluences, can be detected down to fluences of 1.5 J cm^{-2}. The trend of the intensity *vs.* laser fluence, for the sake of discussion, can be subdivided into 4 different phases, as marked in the figure. In phase 1, an increasing trend of the emission intensity is evident, up to laser fluences around 30 J cm^{-2}. Beyond such a threshold, in phase 2, a reduction of the signal is abruptly observed up to fluence values of ∼90 J cm^{-2}. Between 90 and 320 J cm^{-2}, in phase 3, the intensity is low and tends to slowly increase with fluence. Finally, a strong increase of line intensity with the laser fluence is observed again at values higher than 320 J cm^{-2}, in phase 4.

It is important to note that such behaviour can not be produced by the self absorption of lines, since it is also observed
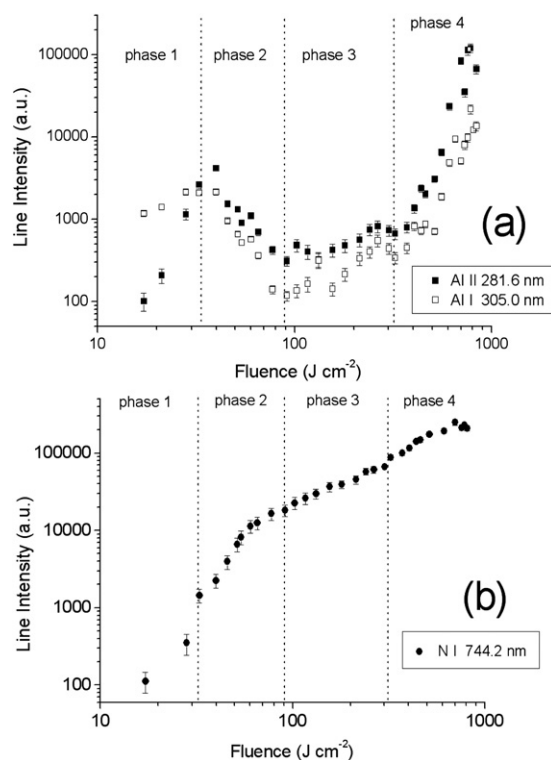

Fig. 1 Trend of integrated intensity with laser fluence of (a) Al II 281.6 nm and Al I 305.0 nm; (b) N I 744.2 nm. The reproducibility of the values for both the lines is in the range 5–20% depending on the laser fluence.

for emission lines deriving from electronic transitions between very high energy levels (*e.g.* Al II 466.3 nm or Al II 358.6 nm), which show very low self-absorption effects.

A different trend was observed for lines emitted by atoms coming from the surrounding environment, such as nitrogen and oxygen. In that case, as shown in Fig. 1b for N I 744.2 nm line, an increasing trend is observed all along the fluence range.

In order to investigate on such trends, it is necessary to determine how the plasma thermodynamic parameters (in particular the temperature) and the total amount of emitting atoms in the plasma affects the plasma emission. This task is afforded in the next sections, by calculating from the spectra the space-averaged temperature, the space-averaged electron density and the total atomized ablated mass in the plasma. All these parameters are calculated by assuming that the plasma is spatially homogeneous in composition and temperature. In reality, it is well known that the spatial gradients of temperature are strong and can be significant[21] and that the buffer gas atoms and target atoms are differently distributed in the plasma.[22] In order to obtain space resolved spectra, an Abel inversion algorithm should be applied to the original spectra as elsewhere shown;[23,24] however, this procedure would result in a strong reduction of the signal to noise ratio, which could not allow an accurate determination of the parameters we are interested in for all the laser fluence used. Mainly for this reason, we thus decided to work with averaged quantities, being confident that the obtained trends can be nevertheless useful to draw a qualitative picture of the analysed processes.

Thermodynamic parameters investigation

The spatially averaged electron density was calculated by measuring the Stark broadening of the Balmer H_α line, according to the formula[25] $n_e(\text{cm}^{-3}) = 8.02 \times 10^{12} (\Delta\lambda_{1/2}/\alpha_{1/2})^{3/2}$ where $\Delta\lambda_{1/2}$ is the FWHM in Angstrom and $\alpha_{1/2}$ is a coefficient, weakly dependent on electron density and temperature, tabulated by Griem.[26] Hydrogen emission is always present in the LIBS spectra taken in ambient air, because of the water vapor due to the natural humidity of the air, which is in part adsorbed on the target surface. In a recent paper,[27] we have shown that the emission profile of the H I line is overlapped to that of the species ablated from the target, rather than to the profiles of N and O emission. This observation supports the validity of the measurement of the Stark broadening of the H Balmer α for determining the electron density in the plasma.

The plasma temperature was also calculated, in the framework of the local thermal equilibrium (LTE) approximation, using the Saha–Boltzmann plot method, as described in ref. 28. This method consists of a generalization of the Boltzmann plot which takes into account both neutral and ionized lines, through the application of the Saha equation and using the values of plasma electron density previously calculated. The lines used for temperature calculation were Al I 305.0, Al I 305.7, Al II 281.6 and Al II 358.6 nm. The Al II 358.6 is a multiplet formed by 3 lines which are not resolved; then the A_{ki} used for building the Saha–Boltzmann plot is an effective value calculated by combining the spectroscopic parameters of these lines. Using the Saha–Boltzmann approach, the maximum difference between the upper level energies of the transitions considered is $\sim$110 000 cm^{-1}, bringing to a considerable reduction of the fitting error with respect to the usual Boltzmann plot method. In this way, the accuracy of the determination of the absolute value of the temperature is of the order of 10%. However, the scatter of the values due to the reproducibility is markedly lower, of the order of 1–3% depending on the laser fluence, since it is not affected by the systematic error coming from the uncertainty of A_{ki} coefficients. The calculated values of plasma electron density and temperature *versus* the laser fluence are plotted in Fig. 2. The lower and the upper values of both parameters (obtained at very low and very high laser fluences) are affected by larger errors in the determination of the electron density. At the lowest fluences, the H_α line is hardly detectable, so that the thermodynamic parameters were not calculated. On the contrary, at highest fluences the wide H_α line tends to overlap with the order shape of the echelle spectrometer, increasing the uncertainty of the width determination.

Both the plots of the temperature and of the electron density *versus* the laser fluence show an increasing trend. However, in the case of temperature, a strong increasing trend is present in phase 1, 2 and 4, while a roll-off is visible in phase 3. The behaviour of electron density appears more regular.

Such trends seem not to trace or be able to explain the trends of intensity, as shown in Fig. 1a; in particular a strong discrepancy is evident in the region around 40 J cm^{-2}, where a strong plasma emission is associated to a quite low plasma temperature. For that reason, we expect that the role of the ablated mass must be determinant.
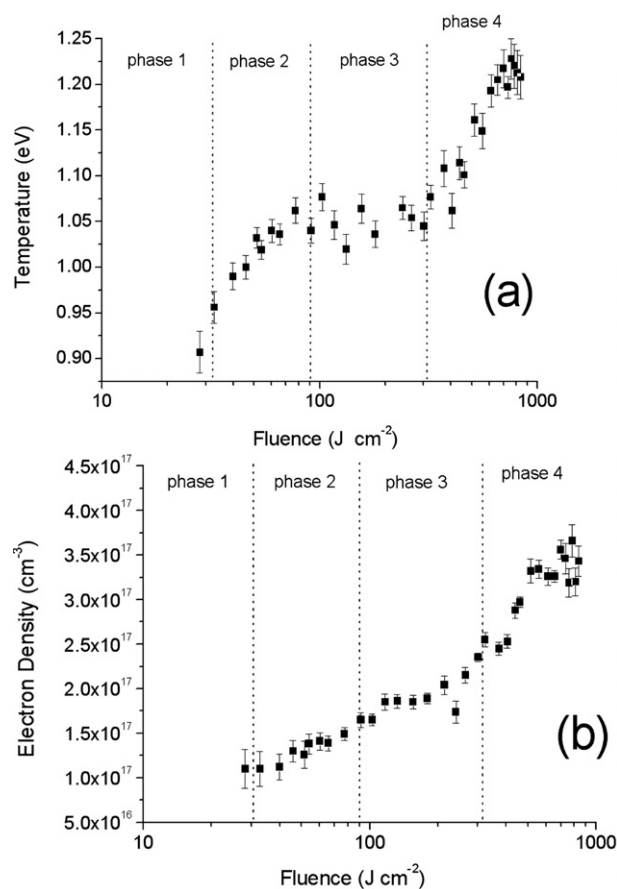

Fig. 2 Trend of plasma temperature (a) and electron density (b) with respect to laser fluence. The scatter of the T values is the order of 1–3%, depending on the laser fluence, while that on n_e is in the range $\sim$2–15%.

Atomized ablated mass

Quantifying the ablated mass in the plasma is not a trivial task. Three different methods can be used to achieve information about it, *i.e.* the measurement of crater dimensions, the spectroscopic estimation of the atomized mass and finally the weighing of the sample. A direct measurement of crater dimensions is undoubtedly useful information but this approach doesn't provide the measure of the mass atomized in the plasma. In fact, the volume of the laser induced crater is often comparable to that of the rim around the hole;[29] moreover, the density of re-condensed or splashed matter in the rim has a different atom density with respect to that of the original target. Then, the calculation of the removed mass as the difference between such volumes leads to large uncertainties. Furthermore, even a precise measure of the removed mass would not be able to discriminate between the mass atomized in the plasma and that ejected (and spectroscopically lost) in particles or large clusters. On the other hand, an estimation of the atomized mass in the plasma, scaled by an arbitrary factor, can be obtained *via* spectroscopic measurements. However, this approach is also strongly affected by the uncertainties in the determination on the thermodynamic parameters and by the geometry of signal collection in the experimental setup. The third approach is the most direct but it is hindered by the low effective ablation rate, which can be much

lower than a μg per pulse. In fact, the mass to be measured is much lower than that corresponding to the resulting crater, since, as mentioned above, the volumes of the crater and of the rims are often comparable. Thus, this approach is possible but it implies the weighing of the sample after a large number of laser shots, as in ref. 30.

In this work, the first and the second approaches were used, which give complementary information about the mass removal, as described in the discussion section.

The method used to calculate from the spectra the total number of atoms of aluminium present in the plasma, i.e. the atomized ablated mass, (scaled by an arbitrary constant factor) was already introduced in ref. 31.

It assumes that the plasma is in local thermal equilibrium in the observation gate, that the plasma is homogenous and that the emission from all the regions of the plasma is collected in the spectrometer without any spatial selection.

In this hypothesis, the lines emitted by a species s (in our case Al I and Al II) can be represented in a Boltzmann plot, according to the linear relation $y = mx + q_s$. Such quantities are defined as $y = \ln(I_{ki}/g_k A_{ki})$, $x = E_k$, $m = -1/k_B T$ and $q_s = \ln(N_s F/U_s(T))$, where I_{ki} and A_{ki} are the integrated intensity and the transition probability of the line, E_k and g_k are the energy and the degeneracy of the atomic upper level of the transition, k_B is the Boltzmann constant, T and $U_s(T)$ are the plasma temperature and the partition function at such temperature and N_s is the number of atoms of the species present in the plasma. The coefficient F is an experimental factor which includes information about the efficiency of the detector and the geometry of the signal collecting system.

It is assumed that the F factor is the same for atomic and ionized species (which corresponds to the hypothesis of homogenous plasma) and that it is the same for all the laser fluences. This hypothesis is valid if the emission from all the regions of the plasma is collected in the spectrometer without any spatial selection; moreover, it is needed that the dimensions of the plasma are much lower than the distance plasma-optical collection system (i.e. the optical fiber tip), so that the solid angle of signal collection for each particle in the plasma is the same. The choice of the collecting system in our experimental setup was determined to respond to these requirements.

In these hypotheses, the measurement of the plasma volume is not necessary and the total number of atoms of aluminium present in the plasma (scaled by the F factor) can be calculated by using the formula

$$N_{TOT} = U_I(T)\exp(q_I) + U_{II}(T)\exp(q_{II})$$

where the subscripts I and II refer to the atomic and ionic aluminium and the q-parameters are determined by fitting the emission lines plotted in the Boltzmann plane.

The atomized ablated mass, calculated from the spectra, versus the laser fluence is reported in Fig. 3. The trend qualitatively traces that of the integrated line intensity, except that in phase 1; in that case, since the temperature of the plasma is evidently very low, a larger number of atoms is needed to produce the signal observed. The behaviour of ablated mass, to some extent unexpected, shows that the ablation process is much more effective in producing atomized mass at laser pulse energies lower than 25 mJ
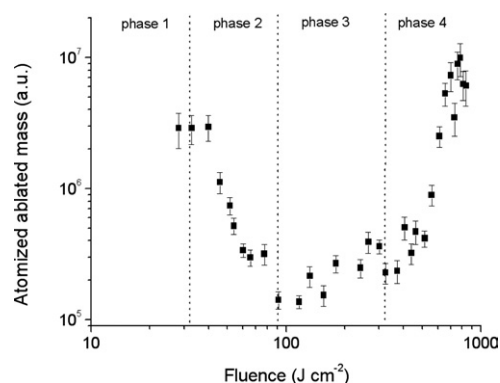

Fig. 3 Atomized ablated mass vs. laser fluence used. The error bars in the Figure, which represent the scatter due to the reproducibility, are of the order of 10–25% of the plotted value depending on the laser fluence.

(corresponding in our case to fluences lower than ∼90 J cm⁻² and higher than ∼180 mJ (corresponding to fluences higher than ∼400 J cm⁻²) than at intermediate values.

Since the ablation efficiency strongly varies with the energy delivered by the laser, it is reasonable that the composition of the plume, mainly formed by ambient air and target atoms, would also dramatically change. The calibration free method, elsewhere presented in detail,[32,33] allows an estimation of the composition of the plume, by using the plasma thermodynamic parameters calculated above and the values of the integrated intensity of non self-absorbed lines of Al, N and O. Since a different spatial distribution of Al and N/O atoms is present in the plume, a considerable uncertainty can be present in the calculated composition, if the plasma is far from being homogenous in temperature and electron density distributions. However, the calculated values are still qualitatively important to understand the evolution of the ablation process with increasing the laser fluence.

The Al lines utilized for the calculation are the same already used for the temperature determination; for the air elements, the N I triplet around 744 nm and the O I triplet around 777.3 nm, were selected. In Fig. 4, the percentage content of N and O atoms in the plume is plotted versus the laser fluence. The Figure seems to be the mirror image of the plot in Fig. 3, showing that in the fluence range between 80 and 500 J cm⁻² (which roughly corresponds to phase 3) the plume is formed at 99% by air atoms.
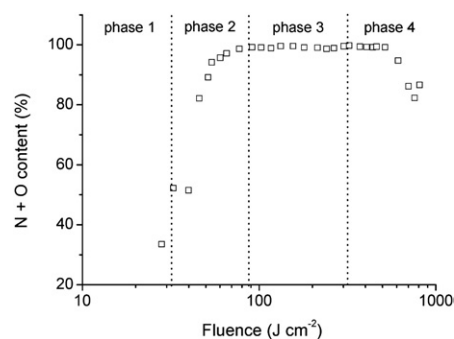

Fig. 4 Percentage content of air atoms in the plume.

Crater analysis

For obtaining information complementary to the spectroscopically determined atomized ablated mass, a direct analysis of the craters on the target surface was also performed.

Residual craters were observed down to laser energies much lower that those shown in the figures of the previous sections, because of the absence in the spectra of Al I 305.0 nm and Al II 281.6 nm lines at fluences below 17 J cm^{-2}.

In Fig. 5 the images and profiles of four craters produced by laser pulses of different energy are shown. Their shapes and profiles are representative of the craters produced in the four phases of laser fluence considered. As evident, the shape of the laser-induced crater changes dramatically with increasing the laser fluence. The different phases can be more clearly evidenced by plotting the trends of the depth (Fig. 6) and of the diameter (Fig. 7) of the crater.
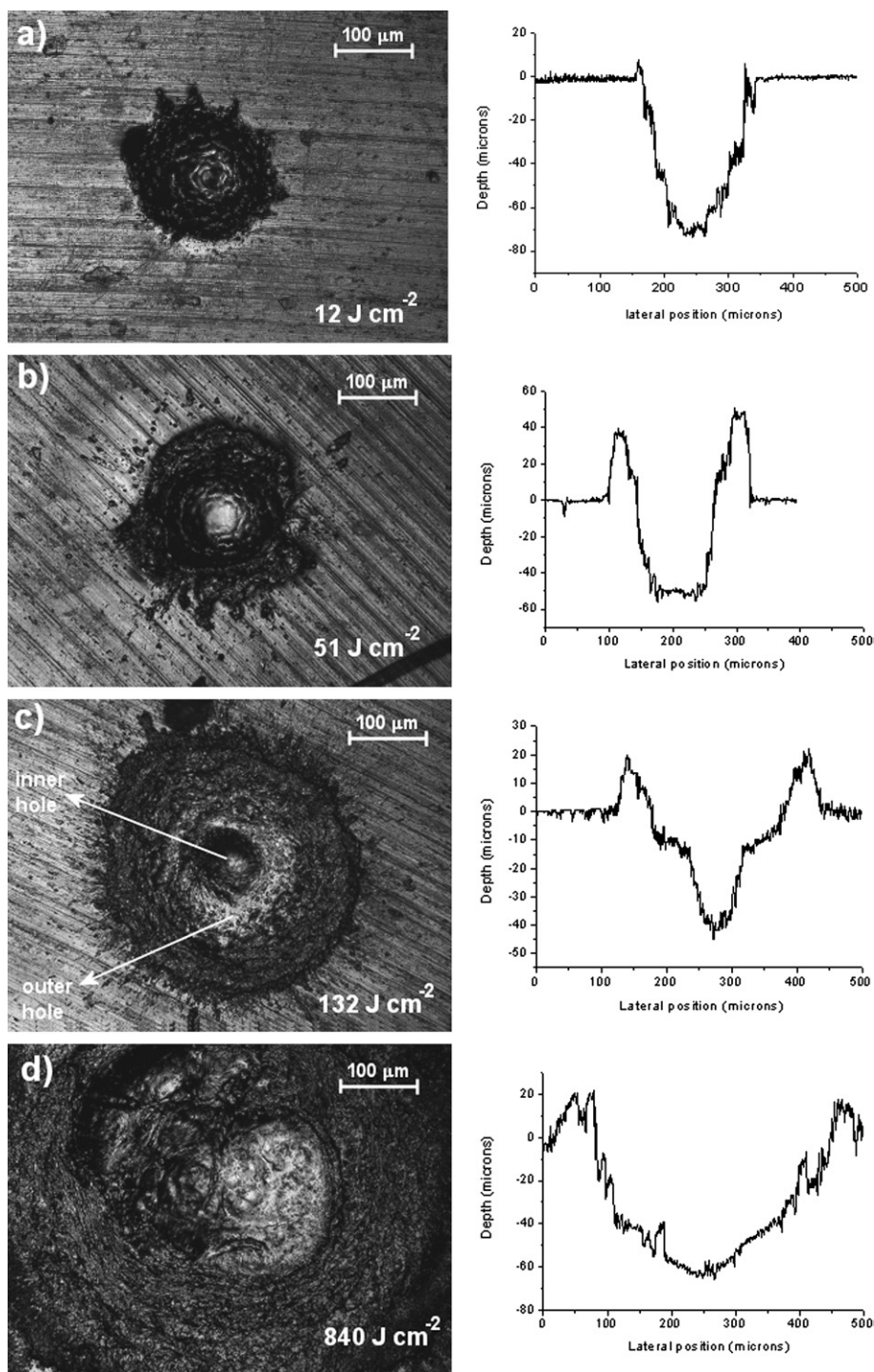

Fig. 5 Images and profiles of craters produced by laser pulses of energy and fluence, respectively, (a) 4 mJ and 12 J cm^{-2}; (b) 16 mJ and 51 J cm^{-2}; (c) 42 mJ and 132 J cm^{-2}; (d) 270 mJ and 840 J cm^{-2}. The craters result from delivering 20 shots on the same spot.

This journal is © The Royal Society of Chemistry 2008

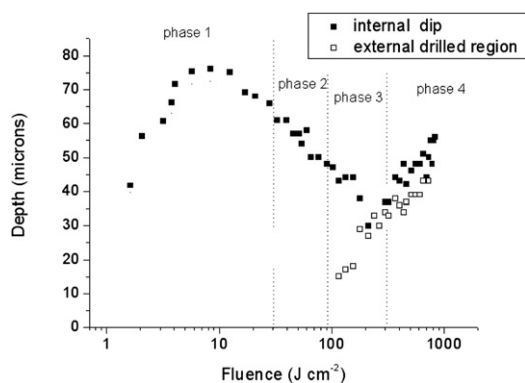*J. Anal. At. Spectrom.*, 2008, **23**, 1518–1528 | 1523

Fig. 6 Trend of the depths of the internal hole and the external drilled area in the crater.
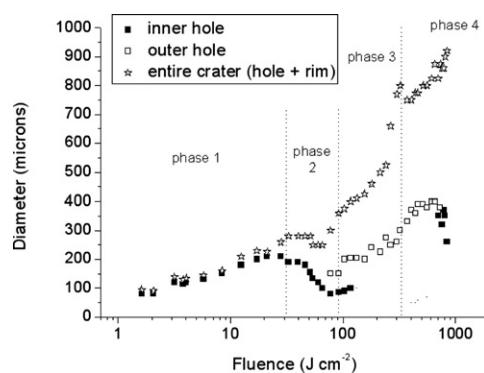

Fig. 7 Trend of the diameters of the internal hole, of the external drilled area and of the entire crater.

Given the complexity of the structure of the crater, it becomes very difficult to calculate the amount of material removed from the target. However, by using the depth and the diameter and by approximating the crater shape as a semi-ellipse, it is possible to obtain an estimation of the volume drilled under the target surface, as plotted in Fig. 8. Such estimated volume is just indicative; in fact, to obtain the real amount of the removed mass (including not only its atomized component but also that dispersed in clusters), the mass accumulated in the rim should be subtracted by that drilled in the hole.
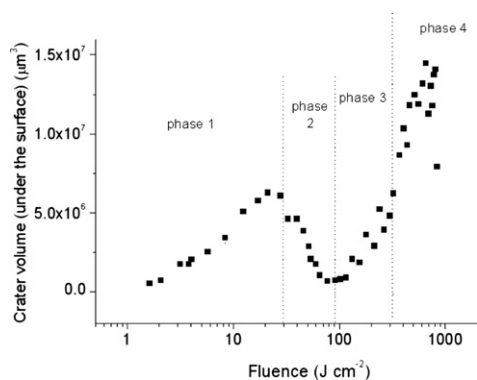

Fig. 8 Estimation of the drilled volume of the crater.

In order to obtain an estimation of the ratio of the volume V_{up} of material accumulated in the rim to the volume V_{down} of the hole, an accurate reconstruction of the 3D structure of the crater was done for a reduced number of laser fluences distributed in the range analysed. The 3D map was obtained by the analysis software distributed with the microscope, which interpolated the stacks of high resolution optical sections of the crater. It is worth to note that V_{up}/V_{down} ratio reaches values higher than one, as elsewhere observed,[29] since the atom density of recondensed material can be lower than that of the original target.

At low energies (phase 1), the crater is characterized by a deep hole in the target surface; a negligible to small rim of re-solidified material is evident around it, resulting in a low V_{up}/V_{down} ratio. The depth of the hole progressively increases up to ~8 J cm^{-2} and then rapidly decreases down to values 2–3 times lower than the peak value. Its diameter increases monotonically reaching a maximum value at the end of phase 1.

In phase 2, both the depth and the diameter of the hole progressively decrease while a surrounding rim formed by melt flushing progressively gets higher and thicker with increasing the laser fluence; these effects result in an abrupt growth of the V_{up}/V_{down} ratio.

In phase 3, a large drilled region forms around the internal hole. In this phase, two concentric holes are visible: an inner one, which progressively reduces in depth and diameter, and an external one, larger and progressively deeper. Around the outer hole a thick rim gradually becomes wider. This structure is clearly visible in the image and in the profile in Fig. 4c.

Increasing the laser energy (phase 4), for fluences higher than ~300 J cm^{-2}, the depth of the crater begins again to increase, while the V_{up}/V_{down} ratio falls down. The complex structure of the crater, formed by two concentric holes, tends to disappear, while its diameter tends slightly to reduce. On the contrary, the whole dimensions of the crater (hole and rim) grow, reaching values around 1 mm. At a fluence around 800 J cm^{-2}, the double-hole structure is no more visible and the crater is irregular with dips and spikes.

Discussion

The trend observed for plasma emission with respect to laser fluence is important both for modelling the process of laser ablation in air and for practical purposes. Comparing Fig. 1a, Fig. 3 and Fig. 8, it is evident that the observed intensity is correlated qualitatively to the amount of atoms present in the plume as well as to the dimensions of the crater. The entire range of laser fluences can be subdivided in four ranges where different regimes of laser ablation seem to occur.

Phase 1

Several methods for determining the threshold fluence for the plasma onset have been published; here, as in ref. 34 it was defined as the minimum fluence needed to detect an emission signal from the Al I doublet at 394.4–396.1 nm, which are found to be the strongest aluminium lines in the spectrum at all the fluences used. The detection relied on the criterion signal-to-noise ratio >3, where the signal was the line peak value and the

noise was the standard deviation of the noise distribution, evaluated in a region of the spectrum adjacent to the observed line. The value obtained is $\sim$1.5 J cm^{-2}, corresponding to a laser energy of $\sim$500 μJ and to a laser irradiance of 1.5×10^8 W cm^{-2}. The threshold value here obtained is similar to the 1.01 J cm^{-2} fluence threshold found by Cabalin and Laserna[34] for a 1064 nm laser pulse focused onto an aluminium target. At fluences lower than 1.5 J cm^{-2}, melting is visible on the target by microscope imaging and vaporization occurs; however, no line emission is detected by the spectrometer since the temperature of vaporized matter is too low. Above the value of 1.5 J cm^{-2}, the crater drilled shows an abrupt growth jumping to an ablation rate of about 2 μm per pulse and the matter removed from the target reaches a temperature, estimated around 5600 K by Sankaranarayanan et al.,[35] at which it is no more transparent to laser photons. Part of the laser energy is then absorbed by the ablated material originating the breakdown of gas and the rapid growth with time of plasma temperature and electron density. From this fluence on, plasma shielding is present in the ablation process and is expected to have much more importance with the increasing of the laser pulse energy. The mechanisms of laser absorption in the plasma are electron–ion (e-i) and electron–neutral (e-n) inverse Bremsstrahlung (IB) and photoionization of excited atoms; however, at a laser wavelength of 1064 nm the e-i IB is dominant,[36] except maybe at very low laser fluences where the plasma is only weakly ionized. The onset of plasma shielding agrees, in order of magnitude, with other works in the literature, though they refer to different laser conditions. As an example, Mao et al.[37] found a threshold of plasma shielding on a copper target in Ar gas around 0.3 GW cm^{-2}, using an excimer laser working at 248 nm, for which a lower absorption is expected with respect to 1064 nm wavelength.

In the fluence range between 1.5 and 8 J cm^{-2}, however, the depth of the crater (Fig. 6) increases with laser energy, denoting that the plasma shielding is modest. Here the plasma is formed almost exclusively by Al atoms and is weakly ionized. In these conditions the n-e IB mechanism can be dominant with respect to the i-e IB mechanism, implying that the plasma shielding is still moderate.

At a fluence around 8 J cm^{-2} the crater depth reaches its maximum value and hereafter begins to decrease, evidence that the laser absorption by the plasma is no more negligible. The plasma formed is now fully ionized, so that the i-e IB mechanism becomes dominant. In this case the absorption coefficient grows more rapidly with time and the laser absorption is much more effective. On the other hand, the external corona of the laser beam continues to reach the entire target surface, so that the diameter of the crater continues to grow up to fluences around 20–30 J cm^{-2} (Fig. 7). Considering both these effects, the maximum volume of the crater is obtained around 20 J cm^{-2} (Fig. 8).

In this fluence range, close to the plasma threshold, it is expected that melt displacement and melt expulsion are negligible in crater drilling. However, Fishburn et al.[38] and Bleiner et al.[14] found that melt displacement is dominant in the ablation of aluminium even at low laser fluences.

In our measurements, the crater shows a small rim around the drilled region, denoting that melt displacement is present but still not much effective. Conversely, melt displacement clearly occurs and becomes important near the end of phase 1, where the
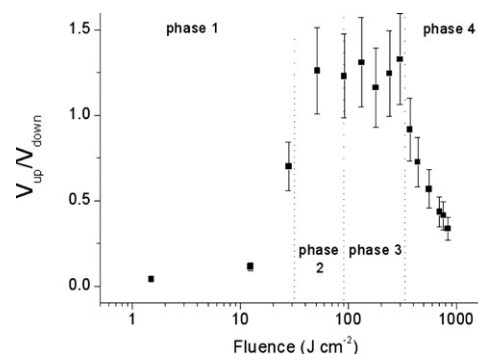

Fig. 9 Ratio of the volume V_{up} of material accumulated in the rim by the volume V_{down} of the hole. The error bars represents 20% of the values.

V_{up}/V_{down} ratio begins to grow (Fig. 9). From these observations, it descends that the drilling must be generated by other ablation mechanisms, namely vaporization or phase explosion. The ablation rate calculated here for phase 1 is in the range between 2 and 4 μm per pulse, far from the typical values of some tens of nanometres estimated by the Hertz–Knudsen equation for normal vaporization of metal targets; Bleiner et al.,[14] using a detailed model of laser vaporization ($\lambda = 266$ nm, fluence = 1 GW cm^{-2}), showed that the ablation rate of an aluminium target is even lower than that of other metals, of the order of 0.3 nm per pulse. Thus, the observed ablation rate seems to rule out the preponderance of vaporization among the mass removal mechanisms for fluences higher than 1.5 J cm^{-2}. For what concerns phase explosion, an extensive discussion appeared in literature about its occurrence and its irradiance threshold, reaching no definitive and shared conclusion. The high irradiance threshold found by Yoo et al.[39] for the occurrence of phase explosion on a silicon target ($\sim$22 GW cm^{-2} by using a 266 nm 3 ns laser pulse, $\sim$420 GW cm^{-2} by using a 532 nm), together with the negligible subsurface heating expected for metals and with the larger size of the critical nuclei predicted for metallic targets,[40] cast doubts on the occurrence of phase explosion of metal targets when irradiated by ns laser pulses. At the opposite, striking evidence of phase explosion occurrence in metals was found[30,41–44] for laser fluences in the range 4–15 J cm^{-2}. In particular, Porneala and Willis,[41] using a Nd:YAG laser emitting 5 ns pulses at 1064 nm, found evidence of phase explosion on an aluminium target both by measuring a jump in the ablation rate at 5.2 J cm^{-2} and by observing a violent ejection of droplets with a shadowgraphic technique. In their work, the plasma is formed successively at a fluence of 5.8 J cm^{-2}. Bearing in mind such results, we can hypothesize that the high ablation rate reported above is originated by a phase explosion already at a few J cm^{-2} fluences. Conversely, at fluences lower than $\sim$1.5 J cm^{-2}, where the crater depth becomes lower than the instrumental resolution ($<$1–2 μm, corresponding to ablation rates $<$25–50 nm), only vaporization takes place. When phase explosion occurs, a fraction of the removed matter is ejected as micrometre-size particles, which, in phase 1, are indeed clearly visible to a naked eye as bright sparks.

Phase 2

In the range between 30 and 90 J cm^{-2} (phase 2), the Al lines intensities exhibit an abrupt decrease with the laser fluence,

approximately by a factor 10, as shown in Fig. 1a. On the contrary, the intensity of the lines emitted by nitrogen and oxygen atoms continues to grow. A similar result was previously found by Wang and Man,[45] who observed a decrease of Al emission and a corresponding increase of N emission in the range $(2–9) \times 10^9$ W cm^{-2}, by using a Nd:YAG laser at 1064 nm in air at atmospheric pressure.

A practical implication is that, when operating at atmospheric pressure, an increase of laser fluence beyond a threshold of $\sim$30 J cm^{-2} (which corresponds in our case to pulses of 10 mJ, irradiance 3×10^9 W cm^{-2}) is useless and it can result in a lower plasma emission, unless a very high laser energy is used (in our case, higher than 180 mJ).

The trend of the thermodynamic parameters and, most of all, the estimation of the atomized ablated mass and the direct observation of the craters, show that the fall down of Al line intensities is strictly correlated to the number of emitting atoms present in the plasma. It implies that, beyond a fluence threshold of $\sim$30 J cm^{-2}, the ablation rate of the laser pulse also abruptly falls, rising up again only beyond 200–300 J cm^{-2}. A similar behaviour was found by Stauter et al.[18] who studied the ablation rate of a Q-switched Nd:YAG laser in the fundamental mode on a Si_3N_4 ceramic in the fluence range 4–40 J cm^{-2}; they found an increasing trend of the ablation rate with fluence up to a threshold of 12 J cm^{-2} and a sudden collapse after such value.

The strong effect of plasma shielding in this energy range is probably the cause of this phenomenon. Such a mechanism would also imply a large delivery of energy in the plasma, causing a rapid growth of plasma temperature. This is consistent with the trend of temperature observed in Fig. 2, even if it refers to temporal window 1–2 μs after the laser shot, when the plasma has notably cooled.

In this fluence range, the percentage of air atoms in the plume markedly increases (see Fig. 4), so that at 80 J cm^{-2} N and O atoms constitute $\sim$99% of its composition. The increase of N and O atoms in the plume, together with an increase of the plasma temperature, originate also an increase of N and O line emissions, visible in Fig. 1b.

The strong growth of plasma shielding and the inclusion in the plasma of air atoms suggest that the plasma propagates in the surrounding gas through a laser supported regime, taking place during the laser-plasma interaction, as suggested also by Stauter et al.[18] The laser absorption produces a hot high-pressure plasma, initially composed by aluminium atoms and ions, which drives a shock wave in the surrounding atmosphere. At the same time, energy is transferred to the shell of ambient gas surrounding the vapour plasma by a combination of thermal conduction, radiative transfer and heating by the shock wave. The heated atmosphere gas, initially transparent to the laser radiation, begins to absorb it up to reach the plasma state, following the same history as the vapour. In the fluence range considered here, the prevailing mechanism of energy transfer between plasma and atmosphere should be the shock wave heating, so that the plasma propagation regime should be similar to a detonation mechanism.[46] Bearing in mind such a process, it is also clear why the plasma shielding and, consequently, the ablation rate depends strongly on the ambient gas composition and pressure.

In phase 2, a strong melt displacement occurs, evidenced by the high rim present around the crater border, formed by re-solidified material (e.g. see the crater profile in Fig. 5b); also melt expulsion occurs, as testified by melt droplets splashed on the target surface around the crater. The extent of melt displacement and expulsion indicates that only a part of the matter removed by the target is converted in atomized matter. The abrupt fall of the volume drilled to values comparable to the ones observed at very low laser fluences in phase 1, together with the importance of melt displacement and splashing, suggest that phase explosion tends to disappear or at least to become largely inefficient.

Phase 3

In the fluence range between 90 and 320 J cm^{-2} (phase 3), both the Al and the ambient air emission lines intensities increase very slightly with laser energy (Fig. 1) as well as the atomized ablated mass.

A roll-off of plasma temperature is evident in Fig. 2, which is not immediately explainable. The effect could be explained if the energy supplied to the plasma is used mainly for the dynamic expansion of the plume and for propagating the plasma into the surrounding gas (through a laser supported mechanism), rather than for raising the kinetic energy of the ions.

Comparing Fig. 3 and Fig. 8, it is evident that some differences exist between the plots of the spectroscopically determined atomized matter and of the optically measured crater hole volume. In particular, the growth of such values occurs at different laser fluences. In the hypothesis that the method for estimating the atomized mass is still valid at high laser energy, where the plasma dimensions are larger, the observed separation could be justified if strong melt displacement and expulsion of droplets are present. In this case, a large amount of material removed in the drilling process is not converted to emitting atoms in the plume. Such a hypothesis is confirmed by the high value of the V_{up}/V_{down} ratio (Fig. 9) and by the difference between the diameters of drilled hole and of the whole crater (hole + rim). Melt expulsion is also confirmed by the splashing residues well visible around the crater by using microscopy imaging.

In this fluence range, a wide drilled region around the central hole, much larger than the laser spot on the surface, is evident in the crater profile. From the comparison between Fig. 3 and Fig. 8, the volume of this secondary hole seems not to contribute to plasma mass; instead, such a structure could be originated by a displacement of molten aluminium, then re-solidified in the crater rim. Considering the large width of such a hole, it is likely that the motion of molten material is the effect of a lateral pressure gradient induced by the high pressure plasma above the target surface.

A similar effect was previously seen by Yoo et al.,[47] who studied the ablation process of a high-power nanosecond laser onto a silicon target.

Phase 4

Phase 4 is characterized by a large increase of plasma emission, plasma temperature and atomized mass. However, the crater volume seems to increase much more slightly than the atomized

mass. The reason of such a difference can probably be explained by hypothesizing that the larger removed mass going in plasma atoms is compensated by a strong reduction of melt displacement. This is suggested by the strong decrease of material accumulated on the rim around the crater (Fig. 9). Thus, the results suggest a transition to a different ablation process, where a higher amount of pulse energy is delivered to the target, resulting in an increase of the plasma mass, and a less important role seems to be played by the plasma-target interaction, leading to melt motion. The presence of such a transition seems to be confirmed by the much more irregular shape of the crater, where spikes and valleys are well visible in the hole. The negligible role of plasma-target interaction is evidenced also by the progressive reduction of the internal hole diameter.

A growth of the energy delivered onto the target is possible if a sort of saturation is present in the plasma shielding mechanism at high laser energy. Such saturation was indeed observed by Bindhu et al.,[48] who studied the laser propagation and energy absorption by an argon spark at different gas pressures. Focusing in argon at atmospheric pressure a Nd:YAG laser emitting at 1064 nm and measuring the energy propagating through the plume, the authors found a trend qualitatively very similar to Fig. 1, where the energy transmitted through the plume increase up to ~10 mJ, then decreases and finally begins to increase again for pulse energies higher than ~150 mJ. The mechanism suggested by the authors for explaining the increase of laser transmission at high energies is the onset of a self-regulating regime in the plasma shielding caused by a saturation of the absorption coefficient. Though it is well known that the laser radiation is more effectively absorbed in argon than in air, the energy thresholds found by Bindhu et al. are very similar to those delimitating the phases in this work.

The higher portion of laser energy delivered onto the target surface (and, consequently, the lower portion absorbed in the plasma and in the expanding shock wave) explains why the ratio between Al and N + O atoms in the plasma increases in this phase (Fig. 4).

The abrupt increase of atomized mass can be explained if the higher amount of energy delivered to the target surface drives again or makes much more effective than previously the phase explosion mechanism. In fact, it would result in a large outflow of vapour (together to melt droplets), rising the plasma atomized mass. Though such a hypothesis seems to be in contrast with the weak increase of crater depth, it would be coherent with the irregular shape of the crater (resulting from an explosive-type mass removal mechanism), with the reduction of matter accumulated in the rim and with the increase of plasma temperature. All these features were found by Yoo et al.,[47] who studied the transition to phase explosion on a silicon target.

Conclusion

The mass removal mechanisms occurring during the laser ablation of an aluminium target were investigated in the fluence range between 1.5 and 840 J cm^{-2}. Both a spectroscopic analysis of the plasma emission and a study of the craters produced on the target surface were performed. The temperature and the electron density of the plasma at a temporal window between 1 and 2 μs

after the laser shots were calculated, which allowed the estimation of the atomized mass present in the plume.

Conversely, microscopic analysis of the craters allowed the calculation of the hole volume and the quantification of the material accumulated in the rim around it, as well as a qualitative inspection of the craters profile and appearance.

Comparing the trends of line intensity, of the atomized plasma mass and of the crater volumes, four laser fluence ranges were identified where different mass removal mechanisms seem to occur. In the lowest fluence range (phase 1), going from the plasma threshold (1.5 J cm^{-2}) up to ~30 J cm^{-2}, the plasma emission, its atomized mass and the crater volume increases with laser energy. Phase explosion was the only mechanism able to justify the ablation rate, i.e. 2–4 μm per pulse, found experimentally in phase 1. Conversely, vaporization is thought to be dominant at laser fluences lower than 1.5 J cm^{-2} when the ablation rate becomes lower than 25–50 nm per pulse. Melt displacement begins to be relevant toward the end of phase 1. In phase 2, going from ~30 to ~90 J cm^{-2}, the trends of plasma emission, of plasma mass and of the crater volume with respect to fluence exhibit an abrupt fall, probably caused by the plasma shielding effect. In this phase, melt displacement and expulsion progressively become more relevant. Phase explosion could be inhibited or become less efficient, since, in this range, the ablation rate strongly decreases, despite the increasing melt displacement and expulsion. Phase 3, going from ~90 to ~320 J cm^{-2}, is characterized by a low plasma emission due to a relatively small amount of plasma atoms, which is caused by plasma shielding. However, apparently in contrast with it, a strong growth of crater volume is observed; this effect seems due to the enlargement and heating of the plasma which exerts a pressure on the molten pool producing a strong melt displacement and expulsion.

Phase 4, including fluences higher than ~320 J cm^{-2}, show a large increase of plasma emission, temperature and atomized mass, though accompanied by a modest growth of the crater volume. In our opinion, the results can be explained if plasma shielding begins to saturate, resulting in a larger amount of laser energy available for mass removal and atomization. The reduction of the crater rim volume testifies a reduction of the melt displacement mechanism, which can explain the modest increase of the crater volume. The crater appearance at fluences around 800 J cm^{-2} shows the occurrence of an explosive-type mass removal mechanism; phase explosion can be driven again or become much more efficient, which is in agreement with the observed temperature and signal growth.

References

1 A. V. Gusarov and A. G. Gnedovets, J. Appl. Phys., 2000, **88**, 4352–4364.
2 S. Tosto, J. Phys. D: Appl. Phys., 2003, **36**, 1254–1268.
3 M. Aden, E. W. Kreutz and A. Voss, J. Phys. D: Appl. Phys., 1993, **26**, 1545–1553.
4 F. Garrelie, C. Champeaux and A. Catherinot, Appl. Phys. A: Solid Surf., 1999, **69**, 45–50.
5 T. E. Itina, J. Hermann, Ph. Delaporte and M. Sentis, Appl. Surf. Sci., 2003, **208–209**, 27–32.
6 G. Callies, H. Schittenhelm, P. Berger and H. Hugel, Appl. Surf. Sci., 1998, **127–129**, 134–141.
7 N. Arnold, J. Gruber and J. Heitz, Appl. Phys. A: Solid Surf., 1999, **69**, S87–S93.

This journal is © The Royal Society of Chemistry 2008

J. Anal. At. Spectrom., 2008, **23**, 1518–1528 | 1527

8 Z. Chen and A. Bogaerts, *J. Appl. Phys.*, 2005, **97**, 063305.

9 A. Bogaerts, Z. Chen and D. Bleiner, *J. Anal. At. Spectrom.*, 2006, **21**, 384–395.

10 D. Bleiner and A. Bogaerts, *Spectrochim. Acta, Part B*, 2006, **61**, 421–432.

11 V. N. Tokarev and A. F. H. Kaplan, *J. Phys. D: Appl. Phys.*, 1999, **32**, 1526–1538.

12 M. M. Martynyuk, *Russ. J. Phys. Chem. (Transl. of Zh. Fiz. Khim.)*, 1983, **57**, 810–821.

13 R. Kelly and A. Miotello, *J. Appl. Phys.*, 2000, **87**, 3177–3179.

14 Bleiner, Z. Chen, D. Autrique and A. Bogaerts, *J. Anal. At. Spectrom.*, 2006, **21**, 910–921.

15 Y. Iida, *Spectrochim. Acta, Part B*, 1990, **45**, 1353–1367.

16 W. Sdorra and K. Niemax, *Mikrochim. Acta*, 1992, **107**, 319–327.

17 J. A. Aguilera and C. Aragon, *Appl. Surf. Sci.*, 2002, **196–198**, 273–280.

18 C. Stauter, J. Fontaine and Th. Engel, *Appl. Surf. Sci.*, 1996, **96–98**, 522–527.

19 P. A. Benedetti, W. Evangelista, D. Guidarini and S. Vestri, *US Pat.*, 6 016 367, 2000.

20 P. A. Benedetti, D. Guidarini, G. Cristoforetti, S. Legnaioli, V. Palleschi, A. Salvetti, R. Spiniello and E. Tognoni, *Micron*, 2007, **38**, 104–108.

21 J. A. Aguilera and C. Argon, *Spectrochim. Acta, Part B*, 2004, **59**, 1861–1876.

22 M. Corsi, G. Cristoforetti, M. Hidalgo, D. Iriarte, S. Legnaioli, V. Palleschi, A. Salvetti and E. Tognoni, *Appl. Spectrosc.*, 2003, **57**, 715–721.

23 M. Corsi, G. Cristoforetti, M. Giuffrida, M. Hidalgo, S. Legnaioli, V. Palleschi, A. Salvetti, E. Tognoni and C. Vallebona, *Spectrochim. Acta, Part B*, 2004, **59**, 723–735.

24 G. Cristoforetti, S. Legnaioli, V. Palleschi, A. Salvetti, E. Tognoni and P. Tomassini, *Spectrochim. Acta, Part B*, 2005, **60**, 888–896.

25 J. Ashkenazy, R. Kipper and M. Caner, *Phys. Rev. A: At., Mol., Opt. Phys.*, 1991, **43**, 5568–5574.

26 H. R. Griem, *Spectral linebroadening by plasmas*, Academic Press, New York, 1974.

27 A. De Giacomo, M. Dell'Aglio, R. Gaudiuso, G. Cristoforetti, S. Legnaioli, V. Palleschi and E. Tognoni, *Spectrochim. Acta, Part B*, 2008, DOI: 10.1016/j.sab.2008.06.010.

28 E. Tognoni, G. Cristoforetti, S. Legnaioli, V. Palleschi, A. Salvetti, M. Mueller, U. Panne and I. Gornushkin, *Spectrochim. Acta, Part B*, 2007, **62**, 1287–1302.

29 P. A. Benedetti, G. Cristoforetti, S. Legnaioli, A. Salvetti, V. Palleschi, L. Pardini and E. Tognoni, *Spectrochim. Acta, Part B*, 2005, **60**, 1392–1401.

30 N. M. Bulgakova and A. V. Bulgakov, *Appl. Phys. A: Solid Surf.*, 2001, **73**, 199–208.

31 G. Cristoforetti, S. Legnaioli, V. Palleschi, A. Salvetti and E. Tognoni, *Spectrochim. Acta, Part B*, 2008, **63**, 312–323.

32 A. Ciucci, V. Palleschi, S. Rastelli, A. Salvetti and E. Tognoni, *Appl. Spectrosc.*, 1999, **53**, 960–964.

33 M. Corsi, V. Palleschi, A. Salvetti and E. Tognoni, *Res. Adv. Appl. Spectrosc.*, 2000, **1**, 41–47.

34 L. M. Cabalin and J. J. Laserna, *Spectrochim. Acta, Part B*, 1998, **53**, 723–730.

35 S. Sankaranarayanan, H. Emminger and A. Kar, *J. Phys. D: Appl. Phys.*, 1999, **32**, 1605–1611.

36 A. Bogaerts and Z. Chen, *Spectrochim. Acta, Part B*, 2005, **60**, 1280–1307.

37 X. Mao, W. T. Chan, M. Caetano, M. A. Shannon and R. E. Russo, *Appl. Surf. Sci.*, 1996, **96–98**, 126–130.

38 J. M. Fishburn, M. J. Withford, D. W. Coutts and J. A. Piper, *Appl. Surf. Sci.*, 2006, **252**, 5182–5188.

39 J. H. Yoo, O. V. Borisov, X. Mao and R. E. Russo, *Anal. Chem.*, 2001, **73**, 2288–2293.

40 X. Xu, *Appl. Surf. Sci.*, 2002, **197–198**, 61–66.

41 C. Porneala and D. A. Willis, *Appl. Phys. Lett.*, 2006, **89**, 211121.

42 X. Xu and D. A. Willis, *J. Heat Transfer*, 2002, **124**, 293–298.

43 K. H. Song and X. Xu, *Appl. Surf. Sci.*, 1998, **127–129**, 111–116.

44 H. Domer and O. Bostanjoglo, *Appl. Surf. Sci.*, 2003, **208–209**, 442–446.

45 X. Wang and B. Man, *J. Korean Phys. Soc.*, 1998, **32**, 373–379.

46 R. G. Root, in *Laser-induced plasmas and applications*, ed. J. Radziemski and A. Cremers, Marcel Dekker, New York and Basel, 1989.

47 J. H. Yoo, S. H. Jeong, R. Greif and R. E. Russo, *J. Appl. Phys.*, 2000, **88**, 1638–1649.

48 C. V. Bindhu, S. S. Harilal, M. S. Tillack, F. Najmabadi and A. C. Gaeris, *J. Appl. Phys.*, 2003, **94**, 7402–7407.